Characterizing the functional dynamics of zinc phthalocyanine from femtoseconds to nanoseconds

Janne Savolainen [a,*], Dennis van der Linden [a], Niels Dijkhuizen [a], Jennifer L. Herek [a,b,*]

[a] *FOM Institute for Atomic and Molecular Physics (AMOLF), Kruislaan 407, 1098 SJ Amsterdam, The Netherlands*
[b] *Optical Sciences Group, Department of Science and Technology, MESA+Institute for Nanotechnology, University of Twente, Enschede 7500 AE, The Netherlands*

Abstract

A promising photosensitizer, zinc phthalocyanine, is investigated by means of steady-state and time-resolved pump-probe spectroscopies. Spectrally resolved pump-probe data are recorded on time scales ranging from femtoseconds to nanoseconds. Global analysis yields the excited-state absorption spectra and lifetimes, as well as the pathways and efficiencies of the competing relaxation processes from the initially excited S_1 state. In addition to the expected nanosecond-scale processes of fluorescence, internal conversion and inter-system crossing that follow the generally accepted kinetic scheme, we also resolve ultrafast dynamics. The nature of these fast processes and their implications to the functional pathway involving triplet formation are discussed.
© 2007 Elsevier B.V. All rights reserved.

Keywords: Photosensitizer; Ultrafast dynamics; Energy-flow diagram; Triplet yield; Zinc phthalocyanine

1. Introduction

The functionality of photosensitizer molecules arises from their ability to react with molecular oxygen to produce highly reactive singlet oxygen and other radical species. Among the applications are photodynamic therapy, blood sterilization and sunlight activated herbicides and insecticides [1,2]. A good photosensitizer should have a high absorption cross-section at a wavelength suitable for the application, e.g. the optical window of tissue in photodynamic therapy [3]. Singlet oxygen species are created by the interaction between a photosensitizer in its triplet state and oxygen molecule, hence the quantum yield of the triplet state is a key factor when searching for or designing new photosensitizers. Other important factors include the rate of photodegradation, solubility, and the tendency to aggregate [3].

In the end, the efficiency of all these applications depends on the photophysics of the photosensitizer molecule. Improving the photosensitizer to enhance the functional pathway and suppress loss channels is an attractive route to explore by coherent control experiments using shaped ultrafast laser pulses [4]. In this approach, an optimisation experiment is designed with the goal of finding a pulse shape that will improve the yield of a chosen photophysical process in comparison to that obtained with a transform-limited (i.e. unshaped) laser pulse. Improving the triplet yield, and correspondingly the efficiency of the photosensitizer molecule in generating singlet oxygen, is a clear target for an optimisation experiments on photosensitizers. However, prior to these experiments a detailed understanding of photophysical processes involved in the excited-state deactivation, as well as their manifestation to the transient spectral signals used as feedback in the control experiments, must be acquired. Here, we report transient absorption experiments and detailed global analysis to extract the pathways, spectral signatures and efficiencies of energy flow in a prototype photosensitizer molecule.

Amongst the most promising second-generation photosensitizers for photodynamic therapy (PDT) are the phthalocyanines [1]. In this study, zinc phthalocyanine (ZnPc) is chosen to serve as a model photosensitizer to study the efficiency of the triplet yield as well as other processes occurring after the initial excitation of the chromophore (see Fig. 1). ZnPc has been in clinical trials [5,6], is easy to obtain, stable, produces singlet oxygen with

* Corresponding authors. Tel.: +31206081234; fax: +31206684106.
E-mail addresses: savolainen@amolf.nl (J. Savolainen),
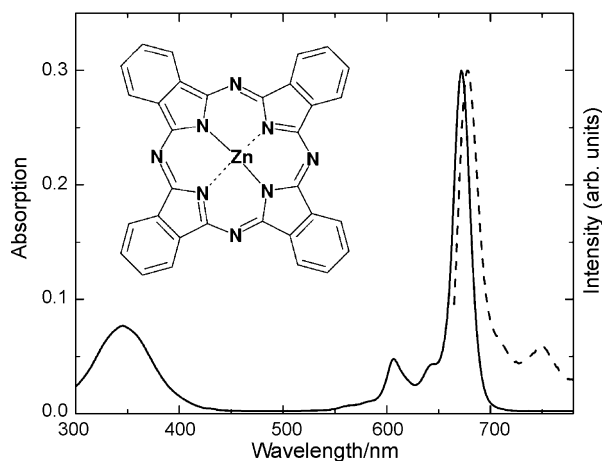j.l.herek@tnw.utwente.nl (J.L. Herek).

Fig. 1. Absorption (solid curve) and fluorescence (dashed) of ZnPc in DMSO. For the latter, the excitation wavelength was 660 nm. Inset: chemical structure of ZnPc.

high yield [7], and has a high absorption cross-section in the far-red part of the visible spectrum close to the optical window of tissue. To fully explore the photosensitising qualities of ZnPc, a detailed description of the intramolecular processes, occurring on time scales ranging from femtoseconds to microseconds, is required. We begin by reviewing results from related studies obtained during the last decade, which we will later compare to our own results.

Several experimental studies on the photophysics of ZnPc and similar compounds (derivatives or different metallophthalocyanines) in solution have been reported [8–19], but so far the results fail to depict a coherent picture of the overall photophysics. The generally accepted energy-flow model includes three major intramolecular relaxation pathways from the initially excited S_1 state. The competition between these processes can be summarized by the modified Gouterman's equation [20]:

$$\Phi_F + \Phi_{IC} + \Phi_{ISC} = 1, \tag{1}$$

where Φ_F, Φ_{IC} and Φ_{ISC} are the quantum yields of fluorescence, internal conversion and inter-system crossing, respectively.

For the most part, first excited-state (S_1) lifetimes (often called fluorescence lifetime (τ_F) due to the direct relation between detected fluorescence intensity and S_1 population) and fluorescence quantum yields, obtained from fluorescence measurements in different environments, are consistent, and similar values are reported in various studies. Measured S_1 lifetimes are in the order of few nanoseconds, for example $\tau_F \sim 2.88$ ns with a quantum yield of $\Phi_F \sim 0.277$ for zinc phthalocyanine tetra sulfonate (ZnPcTS) in DMF [6]. For the sample used in this study, ZnPc in DMSO, a Φ_F of 0.20 ± 0.03 is reported by Ogunsipe et al. [18]. Fluorescence yields and decays of the same order have been reported in different environments like proteins, cell suspensions and in vesicles [21,22], and they are found to be dependent on the surroundings of the chromophore, yet always displaying nanosecond-scale behaviour.

A more complete picture of the nanosecond dynamics is depicted by Bishop et al. in a study of ZnPc (and its 16-deuterated derivative) in toluene by various photophysical methods [23].

The authors report rate constants of 9.1, 38.5, and 5.6 ns, with corresponding quantum yields of 0.34 ± 0.03, 0.08 ± 0.11 and 0.58 ± 0.08 for F, IC and ISC, respectively. However, as an example of the wide variation in the reported nanosecond dynamics, we note a study by Frackowiak et al. These authors found the quantum yield for the inter-system crossing to be even as high as 0.98 ± 0.18 for ZnPc in air-saturated DMSO [12], using a photothermal measurement technique.

The triplet-state lifetime (τ_T) is strongly affected by the presence of molecular oxygen, which drastically reduces τ_T due to efficient intermolecular energy transfer. Grofscik et al. [9] find a τ_T of 220 ± 22 ns for ZnPc in air-saturated ethanol; Lang et al. [22] report 1.6 μs for ZnPcS₃ in aerated aqueous protein solution and 205 μs without the presence of oxygen.

In addition to the nanosecond dynamics described above, also femtosecond and picosecond processes have been reported. The S_1 lifetime of ZnPc in toluene is claimed to be ~35 ps by Rao and co-workers, a value obtained by degenerate four-wave mixing using incoherent light [13]. The setup used, however, was inadequate for quantify components exceeding 100 ps. In addition, the authors report a ~3.5 ps component that is assigned to vibrational relaxation in the S_1 state, as well as a S_n dephasing time of <170 fs. Howe and Zhang report an S_1 lifetime of ~160 ps and an S_2 lifetime of ~10 ps for tetrasulfonated ZnPcS₄ in DMSO [10]. The data were obtained by femtosecond pump-probe measurements, where excitation was to the second excited state. In explaining the multi-exponential behaviour of the kinetics authors introduce an energy-flow model that includes an uphill climb from S_1 to the S_2 state at room temperature and an inverse saturable absorber model. Recently, in a study of artificial light-harvesting complexes where ZnPc is covalently linked to a carotenoid molecule, ultrafast branching of the energy flow in the singlet manifold with time scale of <100 fs has been reported by Berera et al. [24].

Collectively, the various observations from the ultrafast studies suggest that the conventional energy-flow model (Eq. (1)) fails to depict the entire picture of the kinetics, and that faster processes may also play an important role in the photophysics of ZnPc and its derivatives. However, the previous results from the ultrafast studies performed on ZnPc in solution are extremely divergent, and motivate further studies in order to resolve the intramolecular dynamics of this system.

Here, we employ pump-probe spectroscopy from femtosecond to nanosecond time scales in order to deliver a more consistent picture of the kinetic processes following the excitation of the photosensitizer. Using a state-of-the-art pump-probe setup and global analysis of the spectrally broad data we focus on the intramolecular dynamics of ZnPc in DMSO, determining the excited-state spectra, deactivation pathways, time constants and efficiencies. Besides resolving the nanosecond-scale dynamics that follow the conventional energy-level scheme, we show that there indeed are ultrafast processes present. In this context, we also address the role of the solvent, and how solvation dynamics may complicate the analysis of dynamics on ultrafast time scales [25–30]. Global analysis of the temporally and spectrally resolved data allows us to extract a complete picture of the branching ratios between the three competing intramolecular

energy-flow pathways as well as the species-associated spectra (SAS). We present an energy-flow model used in the analysis and discuss the origins of all observed dynamics.

2. Experimental

Steady-state absorbance spectra were measured with a Jasco V-530 spectrophotometer, with the sample in a 1 mm quartz cuvette (Hellma). For the fluorescence measurements, a Jobin Yvon Spex Fluorolog Tau-3 system was used. The fluorescence spectrum and quantum yield were measured by the ratio method [31] using chlorophyll-a in water as a reference sample. Fluorescence lifetimes were measured in the frequency domain using the modulation technique as described in Ref. [32]. Fitting software supplied by the manufacturer was used to obtain the fluorescence lifetime.

The pump-probe setup was as follows: part of the output of an amplified Ti:Sapphire laser (Clark CPA-2001) was coupled into a non-collinear optical parametric amplifier (NOPA), which produced ∼10 μJ near-transform-limited pulses at 672 nm with ∼30 nm FWHM and 22 fs pulse duration (pump pulses). A small fraction of the residual fundamental light was focused to a 2 mm sapphire window to create a white light continuum (WLC) that provides spectrally broad probe pulses ranging from 450 to 710 nm. To avoid any anisotropy effects, the polarization angle between the pump and the probe pulses was set to $54.7°$. The two beams were focused and overlapped at the sample position, where the FWHM of the Gaussian intensity profile of the pump beam was 250 μm. The pulse energy was set to 50 nJ with an adjustable filter, giving a peak power of 3.4×10^9 W cm^{-2} (3.4×10^{14} photons cm^{-2}). The sample was circulated in a 1 mm quartz flow-cell to provide a fresh sample for every pulse to avoid sample degradation or accumulation of long-living states. The probe pulses were coupled into a 35-cm spectrograph with a 256-pixels diode array providing a resolution of ∼1 nm/pixel. Diode signals were read out and AD converted at a rate of 1 kHz to get shot-to-shot statistics.

The time resolution of the pump-probe experiments as well as the amount of spectral dispersion in the WLC was determined by measuring the sum-frequency-mixing signal of the pump and probe pulses at the sample position in a 25 μm thick BBO crystal. The wavelength to be mixed from white light continuum was selected by tuning the phase matching angle of the crystal; in this way, the mixing of different wavelengths of the WLC could be measured. The time resolution was ∼70 fs across the spectrum, and the overall time delay between the blue and red parts of the WLC spectrum (chirp) was approximately ∼300 fs. The measured chirp curve was used to remove the WLC dispersion from the data prior to analysis.

ZnPc and DMSO were both purchased from Sigma–Aldrich and used without further purification. The optical density used in the pump-probe experiments was 0.3 at 672 nm in a 1 mm path-length flow cuvette, giving a concentration of ∼12.6 μM (according to $\varepsilon = 2.38 \times 10^5$ mol^{-1} cm^{-1}, reported by Ogunsipe et al. [18]). To check for any sample degradation, the steady-state absorption spectrum was measured before and after the measurements. No changes in OD or spectral shapes were observed,

indicating sample stability. All measurements were performed on aerated sample at room temperature.

2.1. Data analysis

The temporally and spectrally resolved data were analysed globally using software developed in-house, in which the measured 2D-surface is described by a spectro-temporal model. The model comprises parameters for the initial distribution of population (states (de)populated by the laser), rate constants connecting the states and SAS belonging to the states. The ground-state bleach signal is described by inverting the measured absorption spectrum, leaving only its amplitude to evolve as a free parameter. In a similar manner, the stimulated-emission signal was fitted using the inverted fluorescence spectrum that was scaled with a factor of ν^3. In the fit this spectrum had its amplitude and spectral position as free parameters. The spectral profiles of all other SAS were described by 50 free parameters, which independently represented spectral amplitudes of every 5th pixel. A spline interpolation was made between these points; hence, no assumption on spectral shapes was made. A small weighting factor, based on the second derivative of the spectra, was used to favour smooth spectral shapes.

The fitting makes use of an evolutionary learning loop, where the target objective is to find the physical model that, together with corresponding rate constants, best fits the data. The quality of the fit is evaluated by its χ^2 value. The program employs an algorithm based on evolutionary principles. We start with a generation of 20 random sets of parameters, corresponding to 20 simulated surfaces which are each compared to the measured data to determine a χ^2 value. The best-fitted surfaces are then used to create a new generation of parameter sets. The loop is then let to iterate until convergence to an acceptable χ^2 value is reached and the measured data are simulated sufficiently. Details of the fitting program and examples will be presented elsewhere.

For the time-window 0–7 ps we also made use of standard single time-trace fitting at the selected wavelengths. The fine features at the early times have low amplitudes and the global-analysis program failed to resolve them adequately. In the single trace fitting a sum of exponentials was used as the fitting function. The errors in the resolved time constants (and quantum yields) were determined using the variance in several fits resulting in comparable χ^2 values.

3. Results

3.1. Steady-state and fluorescence measurements

The steady-state absorbance spectrum of ZnPc in DMSO is shown in Fig. 1. The Q-band (S$_0$→S$_1$) has a sharp maximum at 672 nm [33], as well as a vibrational progression to the blue side with a shoulder at 645 nm and a small peak at 606 nm. The shape of the Q-band spectrum and the positions of the absorption maxima indicate that the ZnPc sample is in a monomeric form [18]. Further in the ultraviolet, the Soret or B-band can be seen ($\lambda_{max} = 345$ nm), which we label the S$_0 \to$ S$_2$ transition.

The fluorescence spectrum (Fig. 1, $\lambda_{ex} = 660$ nm) shows an almost perfect mirror image of the absorption spectrum in the Q-band region, including the vibrational progression. The maximum of emission at 680 nm corresponds to an 8 nm Stokes shift. The fluorescence quantum yield was determined to be 0.34 ± 0.2. Retrieval of the lifetime components, according to the modulation technique used [32], returned only one 3.4 ± 0.2 ns component with substantial amplitude.

3.2. Time-resolved spectroscopy

The 2D-transient surface (Fig. 2) features broad positive excited-state absorption (ESA) bands, superimposed with a deep negative signal, due to the ground-state bleach and stimulated emission (SE). These signals are identified in Fig. 2 where they are most pronounced as Bleach + SE (**A**), $S_1 \rightarrow S_{n1}$ ESA (**B₁**), $S_1 \rightarrow S_{n2}$ ESA (**B₂**), and $T_1 \rightarrow T_n$ ESA (**C**).

Directly upon excitation, an instantaneous bleach is present, as well as other overlapping signals. The negative band originally centred at 672 nm broadens and the centre of mass moves towards the red. This behaviour is explained by a dynamic Stokes shift: the solvent molecules redistribute in response to the new electron distribution in the excited state of ZnPc, which lowers the energy of this state and correspondingly red shifts the SE signal. These dynamics are more clearly demonstrated in Fig. 3 (right panel), where transient traces show a rapidly decaying negative signal on the blue side of the band (668 nm) and rapidly growing negative signal on the red side of the peak of the bleach band (686 nm). The decay is found to be bi-exponential and is fitted with time constants of 250 ± 30 fs and 2.5 ± 0.2 ps. Further ultrafast dynamics can be resolved in other regions of the transient absorption spectrum (Fig. 3, left panel). The initial decays of the ESA bands in the spectral regions 460–490 and 615–645 nm are mono-exponential and can be fitted with a time constant of 450 ± 50 and 250 ± 30 fs, respectively. Likewise, the trace at 532 nm requires a 250 ± 30 fs component, but here with a negative pre-exponential factor (i.e. a rise).
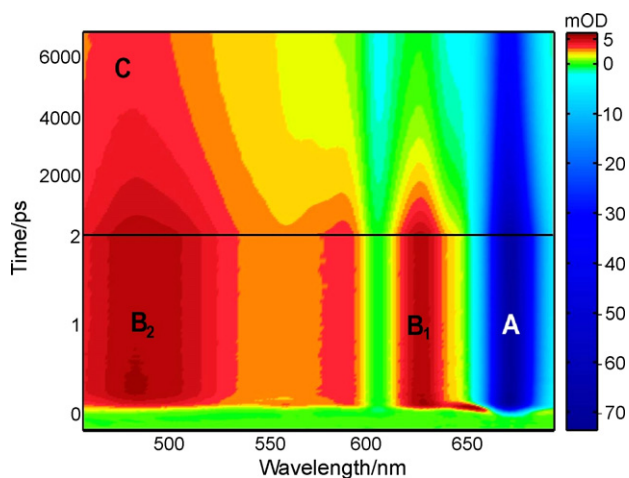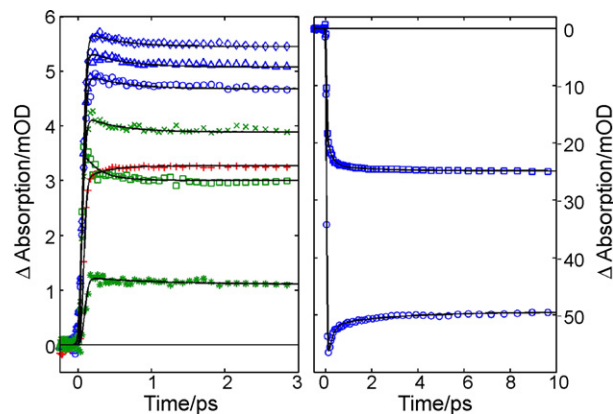

Fig. 3. Early time transient traces (symbols) and fits (solid curves) at selected wavelengths. Left: 466, 472 and 486 nm (circles, triangles and diamonds, respectively) in blue; 532 nm (plus sign) in red; and 612, 620 and 639 nm (asterisk, crosses, and squares, respectively) in green. Right: 668 (circles) and 686 nm (squares) in blue.

In the later time window extending to nanoseconds, the dominating negative bleach band narrows and the centre of mass moves towards the blue, ultimately reaching perfect overlap with the steady-state spectrum ($\lambda_{max} = 672$ nm). The ESA band at ~630 nm decays completely, while below 500 nm the signal persists. Careful inspection of this region shows that maximum, however, is shifted. In Fig. 4, spectral cross-sections reveal that at 7 ps the ESA band on the blue edge of the spectrum has its maximum at 486 nm, while at 7 ns the band peaks at 480 nm. Accounting for the effective fluorescence lifetime (the lifetime of the S_1 state) of 2.9 ± 0.2 ns, and the fact that ISC process must occur on the same time scales to allow for a significant triplet quantum yield, we assign the band in the early time window to the $S_1 \rightarrow S_n$ ESA and the band at later times to the $T_1 \rightarrow T_n$ ESA. Time evolution in this time window across the measured spectrum is shown by time traces at selected wavelengths (Fig. 4, inset).

The late time window of the 2D surface (from 7 ps to 7 ns) can be well fitted according the kinetic model corresponding to

Fig. 2. Pump-probe data as a function of time (*y*) and wavelength (*x*). The characteristic features of stimulated emission and bleach (**A**), singlet ESA (**B₁** and **B₂**) and triplet ESA (**C**) are indicated. Note the two different time windows, and non-linear intensity scaling, used to emphasize the ultrafast dynamics.
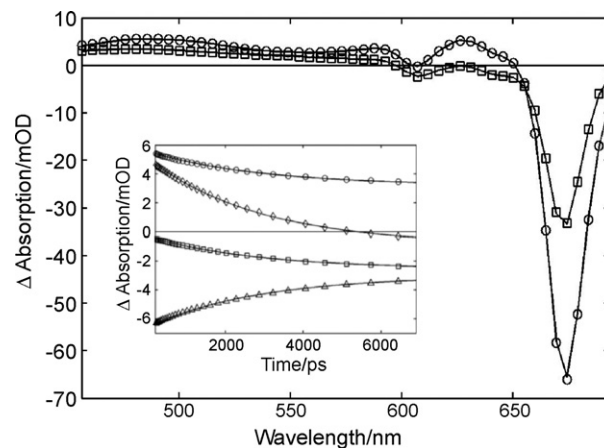

Fig. 4. Transient spectra (symbols) and the fit (solid curves). Time positions: 7 ps (circles) and 7 ns (squares). Inset: selected transient time traces and fits (solid curves) at wavelengths 486 nm (circles), 607 nm (squares), 631 nm (diamonds), and 674 nm (triangles; scaled by 0.1).
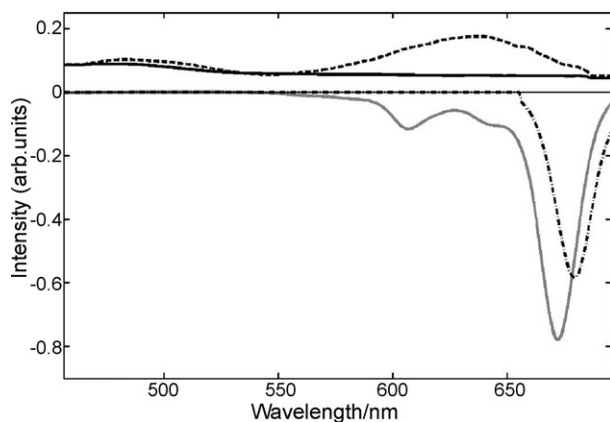
Fig. 5. Resolved species-associated spectra (SAS) from the late time fitting using the model of Fig. 1. S_1 (solid), T_1 (dashed), bleach (solid, grey), and SE (dash-dotted). For comparison see the original combined transient spectra at 7 ps and 7 ns in Fig. 4.

equation 1, in which three competing processes (F, IC and ISC) account for the deactivation of the S_1 state. The resulting SAS are shown in Fig. 5 and quantum yields and lifetimes are given in Table 1. Note that in the global fitting, the depopulation of S_1 is described by two pathways with rate constants K_{ISC} and $(K_{IC} + K_F)$. Hence, in order to resolve all three quantum yields we make use of Eq. (1), the separately determined fluorescence quantum yield [34], and the following three equations:

$$k_F = \frac{\Phi_F}{\tau_F}$$
$$k_{ISC} = \frac{\Phi_T}{\tau_F} \quad\quad (2)$$
$$k_{IC} = \frac{1 - (\Phi_F - \Phi_T)}{\tau_F},$$

wherer k_F is the measured fluorescence rate constant and k_{ISC} and k_{IC} are the rate constants of inter-system crossing and internal conversion, respectively.

From the SAS (Fig. 5) it is clear that the ESA bands are very broad and also overlap the bleach/SE signals. The ESA in the singlet manifold shows two distinct bands peaking around 490 and 640 nm, whereas the triplet ESA has only one clear maximum at about 480 nm. This difference explains the shift of the maximum of the ESA signal in the blue region of the measured spectrum, which is due to the decay of population in the S_1 state, concurrent with the population growth in the T_1 state. The 2.8 ns lifetime of the S_1 state determined from the fit matches well with previous studies [6,15,34], and the effective fluorescence lifetime measured in this study. The position found for the SE spectrum is red shifted by 8 nm, with respect to the peak of the bleach (672 nm), congruent with the Stokes shift found in

Table 1
Lifetimes and quantum yields

	F	IC	ISC
QY	0.28[a]	0.10 ± 0.02	0.64 ± 0.02
Lifetime/ns	10.1 ± 0.3	38 ± 1	4.5 ± 0.2

[a] From Ref. [34].

the steady-state fluorescence measurements. Furthermore, the strong negative signal is first broadened on the red side due to SE and then narrows to the width given by the pure bleach signal when S_1 state is fully depleted.

The ultrafast dynamics observed in the first few picoseconds depict additional processes that cannot be accounted for with such a simple kinetic scheme. Hence, accurate modelling requires a more elaborate description. Bearing in mind that the measured data is a superposition of overlapping signals and that the bleach signal occurs instantaneously, the ultrafast evolution of the transient 2D-surface must be due to excited-state processes, such as energy flow between electronic states, vibrational wavepacket dynamics and/or solvation processes. To better interpret these fast components we refined the kinetic model, as discussed in the following section.

4. Discussion

Based on our global analysis of the data, we aim to update the energy-level diagram of ZnPc. As a caveat, we note that the excited-state absorption bands are very broad and the density of states is high; hence, such a simplistic level scheme is likely inadequate in describing the real molecule in solution. This disclaimer is also important in the assignment of energies to the excited states, which are taken from the maxima of each broad transition. Nevertheless, such a model is a good basis for discussion and is useful in providing organized information, once its limitations are recognized.

The ESA signal from the S_1 state allows us to identify two distinct higher-lying states in the singlet manifold (S_{n1} and S_{n2}, see Fig. 6). S_{n2} is accessed from the S_1 state with probe wavelengths in the range of 460–490 nm, and S_{n1} in the range 615–645 nm. Taking the centre of these ESA bands, we put the energies of these levels at 35,500 and 30,800 cm^{-1} from the ground state. In addition, the observed ultrafast components indicate the presence of short-lived processes involved in the early time dynamics of the system. To our knowledge, these processes have not been previously reported for ZnPc. However, other molecules in DMSO have shown similar dynamics attributed to solvation processes [30].

It is well known that solvation dynamics can occur on several time scales [25–30]. For example, dielectric relaxation (i.e. the Stokes shift) generally takes place in picoseconds, while inertial components of the solvent dynamics occur on femtosecond time scales. Hence, it is no surprise that these different time scales show up also here. The solvation process is nonexponential in nature, and can be characterized only approximately by a set of exponential decay times. In a study of the solvation dynamics of coumarin 153 in DMSO [30], the spectral solvation response function could be fitted with time constants of 214 fs, 2.29 ps and 10.7 ps. The fastest component was assigned to the inertial component of solvation followed by the dielectric nature of the solvation processes. In light of this, we are inclined to attribute the 250 fs and the 2.5 ps components to inertial and dielectric solvation dynamics of the DMSO solvent. The 450 fs time constant, while not directly corresponding to one of the previously determined time constants for DMSO solvation dynamics [30],
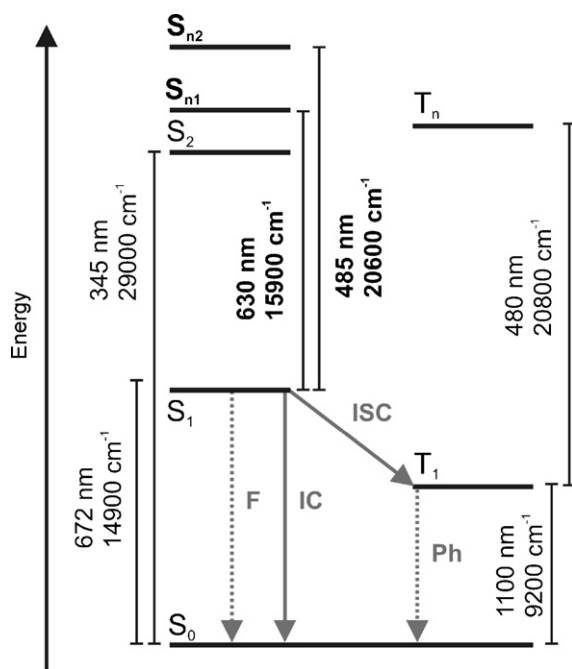
Fig. 6. Schematic of the proposed new energy-level diagram for ZnPc showing both the singlet (S) and triplet (T) manifolds and the deactivation pathways from the S_1 state: fluorescence, *F*; internal conversion, IC; inter-system crossing, ISC; and phosphorescence, Ph. Newly found states and energy spacings are shown in bold.

may also have the same origin. Alternatively, it could reflect intramolecular dynamics occurring in the ZnPc deactivation, such as relaxation or equilibration between energy levels. Likely targets would be the two degenerate Q states in ZnPc, which are spectroscopically indistinguishable upon excitation, or an independent precursor energy level that rapidly decays to the S_1 state. Even though the ultrafast components can be clearly observed in the data over a wide spectral range (see Fig. 3), the fitting program was unable to extract neither unique spectral bands nor connections to other states for these features without substantial initial input and fitting restrictions. Unfortunately, the data offer no decisive evidence for assigning the 450 fs component; nonetheless, the existence of ultrafast dynamics that cannot be explained by the generally accepted energy-flow scheme is evident, and furthermore is not without precedent.

Previous studies fail to paint a clear picture of the ultrafast dynamics of ZnPc. Bearing in mind that some of these studies were on ZnPc derivatives (i.e. tetrasulfonated ZnPc), we nonetheless feel a comparison is worthwhile. Our justification is based on ab initio calculations that indicate the primary photophysics originate from the central conjugated ring structure of the ZnPc molecule [35,36].

Howe and Zhang [10] have suggested a model including an energy-flow equilibrium between S_1 and S_2 states in tetrasulfonated ZnPc. At room temperature, kT is approximately 200 cm^{-1} where as the energy separation between the S_1 and S_2 states is 14,100 cm^{-1} Hence, we find it unlikely that a molecule in the S_1 state could gain enough energy to jump to the S_2 state, or that there could ever be an equilibrium between the two excited states. Furthermore, the 10 ps lifetime for the $S_2 \rightarrow S_1$ inter-

nal conversion seems rather long, especially when comparing to the work by Fournier et al. [14] where a lifetime of <210 fs is reported for the same transition in NiPc and in CuPc. Also problematic here is that the data by Howe and co-workers shows a 160 ps component, which is assigned to the decay from S_1 to the ground state. We find no evidence of this component in our measurements and considering that the fluorescence lifetime is in the order of 3 ns it should simply not be possible to have such a fast decay pathway from the S_1 state.

Using degenerate four-wave mixing with incoherent light, Rao et al. found three different time components [13], which were assigned to phase relaxation of S_n states (<170 fs), vibrational relaxation (~3–5 ps), and population relaxation from the S_1 to the ground state (35 ps). Again, such a fast relaxation from S_1 is unrealistic, considering the known fluorescence quantum yield and lifetime. However, the 3–5 ps found for the vibrational relaxation is of the same order as was found in the present study. Their assignment to a solvation processes is consistent with our resolution of the dynamic Stokes shift.

Berera and co-workers studied ZnPc photophysics in an artificial light-harvesting complex where excitation energy is transferred from the ZnPc to a carotenoid moiety [24]. To explain the ultrafast dynamics observed in this dyad system, they suggest a model that includes branching from an initially excited precursor state to two different S_1 states. The origin for the proposed deactivation scheme is attributed to ground-state heterogeneity. Only one of the S_1 states connects to the triplet state, while the other channel leads to energy transfer to the carotenoid molecule.

The discrepancies in the measured fluorescence lifetimes and quantum yields can likely be explained by sample concentration effects. In this work, the lifetime determined in the fluorescence measurements (3.4 ns) is somewhat longer than was found in the pump-probe measurements (2.9 ns), which is most likely due to the higher concentration used in the pump-probe experiments, leading to self-quenching of the S_1 population and re-absorption of emitted photons. These phenomena are frequently seen in fluorescent molecules with relatively small Stokes shifts and high absorption cross-sections [32]. The lifetimes and quantum yields reported in the literature vary from 2.88 to 3.4 ns and from 0.18 to 0.34, respectively [6,12,17,23]. The cause of this variation likely also stems from the different concentrations and solvents used. In calculating the values for Table 1 we chose to use the fluorescence quantum yield of 0.28 [34], corresponding to the lifetime of 2.88 ns found in this study.

Perhaps the most important photophysical parameter is the quantum yield for triplet formation, which is directly related to the functional photosensitising applications. The found quantum yield of 0.64 ± 0.02 for the inter-system crossing is only slightly higher than reported by Bishop et al. (0.58 ± 0.02) [23], which might be due to the different solvent used. In contrast, a quantum yield close to 1 as reported by Frackowiak et al. seem unrealistically high [12]. It is important to note that the ambiguity of the fluorescence quantum yield discussed above does not affect our determination of the quantum yield of triplet formation, which is resolved directly from the fit of the data with the kinetic model. Hence, the fluorescence quantum yield is only used to calculate the quantum yield of internal conversion process.

Finally, the possible existence of ultrafast intramolecular dynamics and branching in the deactivation of the ZnPc photosensitizer molecule opens new opportunities for coherent-control experiments [37,38]. In further studies, we will explore the possibility to find a laser pulse shape that leads to enhancement of the functional channel in which excitation energy flows to the triplet state. Success would further imply that it is possible to enhance the efficiency of this photosensitizer by means of pulse shaping.

5. Conclusions

We conclude that by combining fluorescence and pump-probe measurements with global analysis of the data we can describe the excited-state dynamics of ZnPc in detail. Once the fluorescence lifetime and quantum yield are known, careful transient-absorption measurements combined with global analyses provide information about the kinetics of the molecular system, ranging from femtosecond to nanosecond time scales. With this, we are able to resolve the lifetimes and quantum yields of fluorescence, internal conversion, and inter-system crossing processes, determine the species-associated spectra belonging to the excited states, and extract dynamics due to solvation. We suggest a new energy model, comprising newly resolved excited states in the singlet manifold accessed by the probe pulse.

Acknowledgements

References

[1] M.C. DeRosa, R.J. Crutchley, Coord. Chem. Rev. 233 (2002) 351.
[2] M. Ochsner, J. Photochem. Photobiol. B 39 (1997) 1.
[3] I.J. MacDonald, T.J. Dougherty, J. Porphyrins Phthalocyanines 5 (2001) 105.
[4] R.S. Judson, H. Rabitz, Phys. Rev. Lett. 68 (1992) 1500.
[5] C.N. Lunardi, A.C. Tedesco, Curr. Org. Chem. 9 (2005) 813.
[6] J.W. Owens, R. Smith, R. Robinson, M. Robins, Inorg. Chim. Acta 279 (1998) 226.
[7] C.M. Allen, W.M. Sharman, J.E. Van Lier, J. Porphyrins Phthalocyanines 5 (2001) 161.
[8] S.M.T. Nunes, F.S. Sguilla, A.C. Tedesco, Braz. J. Med. Biol. Res. 37 (2004) 273.
[9] A. Grofcsik, N. Baranyai, I. Bitter, V. Csokai, M. Kubinyi, K. Szegletes, J. Tatai, T. Vidoczy, J. Mol. Struct. 704 (2004) 11.
[10] L. Howe, J.Z. Zhang, J. Phys. Chem. A 101 (1997) 3207.
[11] L. Howe, J.Z. Zhang, Photochem. Photobiol. 67 (1998) 90.
[12] D. Frackowiak, A. Planner, A. Waszkowiak, A. Boguta, R.M. Ion, K. Wiktorowicz, J. Photochem. Photobiol. A 141 (2001) 101.
[13] S.V. Rao, D.N. Rao, J. Porphyrins Phthalocyanines 6 (2002) 233.
[14] M. Fournier, C. Pepin, D. Houde, R. Ouellet, J.E. van Lier, Photochem. Photobiol. Sci. 3 (2004) 120.
[15] P.S. Vincett, E.M. Voigt, K.E. Rieckhoff, J. Chem. Phys. 55 (1971) 4131.
[16] Q.H. Zhong, Z.H. Wang, Y.Q. Liu, Q.H. Zhu, F.A. Kong, J. Chem. Phys. 105 (1996) 5377.
[17] A. Ogunsipe, J.Y. Chen, T. Nyokong, New J. Chem. 28 (2004) 822.
[18] A. Ogunsipe, D. Maree, T. Nyokong, J. Mol. Struct. 650 (2003) 131.
[19] A. Ogunsipe, T. Nyokong, J. Mol. Struct. 689 (2004) 89.
[20] M. Gouterman, in: D. Dolphin (Ed.), The Porphyrins, Academic Press, New York, 1978.
[21] G. Valduga, E. Reddi, G. Jori, R. Cubeddu, P. Taroni, G. Valentini, J. Photochem. Photobiol. B 16 (1992) 331.
[22] K. Lang, J. Mosinger, D.M. Wagnerova, Coord. Chem. Rev. 248 (2004) 321.
[23] S.M. Bishop, A. Beeby, A.W. Parker, M.S.C. Foley, D. Phillips, J. Photochem. Photobiol. A 90 (1995) 39.
[24] R. Berera, C. Herrero, L.H.M. van Stokkum, M. Vengris, G. Kodis, R.E. Palacios, H. van Amerongen, R. van Grondelle, D. Gust, T.A. Moore, A.L. Moore, J.T.M. Kennis, Proc. Natl. Acad. Sci. U.S.A. 103 (2006) 5343.
[25] R. Jimenez, G.R. Fleming, P.V. Kumar, M. Maroncelli, Nature 369 (1994) 471.
[26] S.A. Kovalenko, A.L. Dobryakov, J. Ruthmann, N.P. Ernsting, Phys. Rev. A 59 (1999) 2369.
[27] S.J. Rosenthal, X.L. Xie, M. Du, G.R. Fleming, J. Chem. Phys. 95 (1991) 4715.
[28] P.J. Rossky, J.D. Simon, Nature 370 (1994) 263.
[29] G.R. Fleming, M.H. Cho, Annu. Rev. Phys. Chem. 47 (1996) 109.
[30] M.L. Horng, J.A. Gardecki, A. Papazyan, M. Maroncelli, J. Phys. Chem. 99 (1995) 17311.
[31] J.N. Demas, G.A. Crosby, J. Phys. Chem. 75 (1971) 991.
[32] J.R. Lakowicz, Principles of Fluorescence Spectroscopy, Kluwer Academic and Plenum Publishers, New York, 1999.
[33] H. Abramczyk, I. Szymczyk, J. Mol. Liq. 110 (2004) 51.
[34] J.W. Owens, M. Robins, J. Porphyrins Phthalocyanines 5 (2001) 460.
[35] K.A. Nguyen, R. Pachter, J. Chem. Phys. 114 (2001) 10757.
[36] G. Ricciardi, A. Rosa, E.J. Baerends, J. Phys. Chem. A 105 (2001) 5242.
[37] M. Shapiro, P. Brumer, Principles of the Quantum Control of Molecular Processes, Wiley, New York, 2003.
[38] J.L. Herek, J. Photochem. Photobiol. A 180 (2006) 225.